Reac Kinet Mech Cat (2015) 115:93–104
DOI 10.1007/s11144-014-0828-6

Thermal decomposition kinetics of carbon nanotubes–the application of model-fitting methods

S. Panic · E. Kiss · G. Boskovic

Received: 30 September 2014 / Accepted: 11 December 2014 / Published online: 7 January 2015

Abstract The aim of this work was to study the nonisothermal oxidation kinetics of as-grown and purified carbon nanotubes and to correlate kinetic parameters to their thermal and textural properties. The kinetic analysis was performed by using the TG/DTG experimental data collected in the temperature range from 25 to 1,000 °C at a single heating rate. The data were fitted by using selected model-fitting methods to find an appropriate kinetic model of decomposition. The determined values of activation energy and pre-exponential factor for the as-grown samples confirm different thermal stability among samples, while the different mechanisms of their decomposition are in accordance with tubes specific textural properties. The kinetic parameters confirmed the oxidative stability evolution of CNTs due to the applied purification treatment, however, only for alumina-based CNTs. The kinetics of the purified sample of silica origin could not be analyzed by any of the selected mathematical methods pointing out to another experimental approach.

Keywords Carbon nanotubes · Purification · Thermal stability · Kinetic analysis · Model-fitting methods

List of symbols

A	Pre-exponential factor (K/min),
E_a	Activation energy (kJ/mol),
T	Temperature (K),
R	Universal gas constant (J/mol K),
t	Time (min),
$f(\alpha)$	Differential reaction model,

S. Panic · E. Kiss · G. Boskovic (✉)
Faculty of Technology, University of Novi Sad, Bul. cara Lazara 1, 21000 Novi Sad, Serbia
e-mail: boskovic@uns.ac.rs

$g(\alpha)$ Integrated reaction model,
m_0 Initial weight of the sample (g),
m_t Sample weight after time t (g),
m_f Final sample weight (g),
n Reaction order
α Conversion fraction
β Temperature gradient

Introduction

In recent years, carbon nanotubes (CNTs) proved to be an excellent material for application in many research fields including electronics, transportation, environmental protection, medicine, etc. [1]. The current implementation of CNTs in most of these fields implies the use of this nanomaterial, not only as a single component, but also as reinforcing phase in order to obtain the complex materials with improved properties [2]. The produced nanocomposites are often exposed to different temperatures and in different gas environments regardless of the application field [3, 4]. In this regard, the study of the thermal stability of CNTs and the kinetics of their decomposition is of great importance. However, to date, studies dealing with this topic are scarce. Besides, kinetic parameter values available in the literature are often different due to various experimental conditions and mathematical methods applied. According to the research of Brukh and Mitra [5], the activation energy of commercial singe-walled CNTs is in the range of 120–140 kJ/mol, while for the multi-walled it amounts $\sim$290 kJ/mol. Illeková and Csomorová [6] confirmed the similar value of the activation energy for commercial singe-walled CNTs ($\sim$120 kJ/mol), while, on the other hand, Vignes et al. [7] showed that the activation energy for commercial multi-walled CNTs is much lower ($\sim$150 kJ/mol). Different values of the activation energies for CNTs in the literature are probably a consequence of their different structural properties, such as: length, diameter, nature of functional groups, the presence of defects and purity of the examined sample [2]. In addition, it was shown that the kinetics of CNTs combustion depends on the sample size and the partial pressure of O_2 in the applied gas mixture [8].

Carbon nanotubes produced by catalytic chemical vapor deposition method contain catalyst particles and non-selective forms of carbon which have to be removed prior to tubes application. The liquid oxidation method, using a proper combination of acids and basis, is often used for the purification. However, the treatment can also cause the changes of some physico-chemical properties of as-grown CNTs and subsequently affect the thermal stability and decomposition kinetics of the purified tubes. According to some authors [9–11], the activation energy and pre-exponential factor of CNTs after purification by liquid oxidation vary depending on the number of formed/removed structural defects and degree of CNTs functionalization. Increasing the number of structural defects during treatment reduces the activation energy [7], while a higher degree of functionalization contributes to the increase of the activation energy due to the presence of

hydrogen bonds formed between functional groups [11]. Since CNTs are subject to various structural changes during the purification, it can be assumed that the thermal decomposition kinetics of the purified tubes is much more complex and the whole process consists of several steps. The rate of each individual step is controlled by different mechanism and characterized by specific values of kinetic parameters [8, 9]. Therefore, the selection of appropriate experimental conditions, as well as mathematical methods for data processing is very important in order to get an adequate description of the complete thermal degradation reaction mechanism and its kinetics.

According to our previous results [12], the synthesis of CNTs over different catalysts (alumina and silica-supported) resulted in nanotubes having similar structural properties, as indicated by TEM, and confirmed by both combustion temperature and heat of combustion in the TPO regime. The efficiency of the applied liquid oxidation method in terms of purification was also confirmed by TG analysis based on the total mass losses of 95 % for both purified CNT samples. On the other hand, the applied purification procedure caused different trends in thermal stability of the tubes grown on different catalysts, revealed as significant changes in the heat of combustion of as is and purified samples. The observed thermal stability evolution was explained as the consequence of the changes in CNTs order degree and morphology upon purification, as well as the degree of functionalization [12]. These results were also confirmed by TEM, XRD and Raman spectroscopy data. In order to extend the thermal properties of the investigated CNT samples, in this paper, the parameters of thermal decomposition kinetics of the same CNTs samples and their textural properties were examined and correlated with the aforementioned results.

Theoretical basis of thermal decomposition kinetics

The rate of thermal decomposition process can be generally expressed as:

$$\frac{d\alpha}{dt} = Ae^{-(E_a/RT)}f(\alpha) \tag{1}$$

During the thermal process, progress of a component decomposition can be followed by its conversion fraction α calculated from the following equation:

$$\alpha = \frac{m_0 - m_t}{m_0 - m_f} \tag{2}$$

A variation of the sample weight values can be revealed from both isothermal and nonisothermal kinetic experiments. Thus, kinetic decomposition parameters, also called "kinetic triplet", can be obtained from the corresponding data of an isothermal experiment using Eq. 1. If the reaction is carried out under nonisothermal conditions, Eq. 1 can be transformed by expressing the reaction rate as a function of the temperature at a constant heating rate:

$$\frac{d\alpha}{dT} = \frac{d\alpha}{dt}\frac{dt}{dT} = \frac{d\alpha}{dt} \cdot \frac{1}{\beta} \tag{3}$$

For which one has to know the reaction rate at both nonisothermal, and isothermal conditions, as well as the temperature gradient, $\beta = \frac{dT}{dt}$.

Substituting Eq. 1 into Eq. 3 gives the differential form of the reaction rate at nonisothermal conditions:

$$\frac{d\alpha}{dT} = \frac{A}{\beta} e^{-(E_a/RT)} f(\alpha) \tag{4}$$

Integrating Eqs. 1 and 4 gives the integral form of the reaction rate at isothermal and nonisothermal conditions, respectively:

$$g(\alpha) = Ae^{-(E_a/RT)}t \tag{5}$$

$$g(\alpha) = \frac{A}{\beta}\int_0^T e^{-(E_a/RT)}dT \tag{6}$$

The study of thermal decomposition kinetics generally begins with the selection of appropriate kinetic models [13]. Thermal decomposition models are classified according to the shape of isothermal curves (α vs. t or $d\alpha/dt$ vs. α), or consistent with the assumed reaction mechanism in the case the reaction is performed at nonisothermal conditions. The first involves increasing, decreasing, linear and sigmoidal models [14]. On the other hand, the mechanistic assumptions based on nonisothermal data recognize the following models: nucleation and growth, geometrical contraction, diffusion and order-based [14].

Once kinetic data are exerted, they can be analyzed by various methods depending on the kinetic data temperature history. In the case they were exerted from a nonisothermal kinetic experiment at a single heating rate, model-fitting methods are convenient. Model-fitting methods are based on fitting the kinetic data to different models, whereby the model giving the best statistical fit is chosen as appropriate to calculate the kinetic parameters– pre-exponential factor (A) and the activation energy (E_a). These methods are classified into isothermal (conventional) method and nonisothermal methods.

The most commonly used nonisothermal model-fitting methods are the following:

The direct differential method [15] uses the differential form of the reaction rate at nonisothermal conditions (Eq. 4). Taking the logarithm of this equation gives a proper linear plot for the kinetic parameters determination:

$$\ln\frac{d\alpha/dT}{f(\alpha)} = \ln\frac{A}{\beta} - \frac{E_a}{RT} \tag{7}$$

The Freeman-Carroll method [16, 17] also uses the linear equation of the reaction rate at nonisothermal conditions Eq. 4, which, by taking the incremental differences in the variables and following several rearrangements, results in the linear equation:

$$\frac{\Delta \ln \frac{d\alpha}{dT}}{\Delta \ln f(\alpha)} = 1 - \frac{E_a}{R} \frac{\Delta \frac{1}{T}}{\Delta \ln f(\alpha)} \tag{8}$$

The last can be extended, however, with a function accounting for pre-assumed reaction order n, whose substitution into Eq. 8 transforms to Eq.9 [16, 17], which is convenient for the reaction order verification:

$$\frac{\Delta \ln \frac{d\alpha}{dT}}{\Delta \ln(1-\alpha)} = n - \frac{E_a}{R} \frac{\Delta \frac{1}{T}}{\Delta \ln(1-\alpha)} \tag{9}$$

The Coats-Redfern method, in contrast to the previous two methods, uses the integral form of the reaction rate at nonisothermal conditions (Eq. 6). Taking into account certain mathematical approximations [18], the Coats-Redfern expression has the following linear form:

$$\ln\left(\frac{g(\alpha)}{T^2}\right) = \ln\left(\frac{AR}{\beta Ea}\right) - \frac{Ea}{RT} \tag{10}$$

Experimental

Carbon nanotube synthesis and purification

Carbon nanotubes (CNTs) were synthesized in the presence of two Fe-Co catalysts differing in supports, Al_2O_3 and SiO_2 [12]. The synthesis was carried out in a home-made quartz reactor setup, as described elsewhere [19]. The obtained CNT samples were labeled according to the catalyst support used for the tubes synthesis: CNTs-A and CNTs-S, for alumina- and silica-originated CNTs, respectively.

In order to remove the catalyst support and remaining metal particles, the raw CNT product was treated with 3 M NaOH and subsequently with 3 M HNO_3 solutions for 6 h reflux at the boiling point of each, with intermediate washing. Finally, the purified CNTs were washed with distilled water, dried at 110 °C for 24 h [20] and labeled as CNTs-A-P and CNTs-S–P.

Characterization of the products

Thermal analysis was carried out using SDT Q600 TA Instruments by means of temperature programmed oxidation (TPO). Measurements were done in the temperature range 25–1,000 °C at a ramping rate of 10 °C min^{-1}, in a 100 cm^3 min^{-1} flow of 5 % O_2/He. The gas mixture was prepared using high purity gases, and the flow rate was controlled by a mass flow controller integrated into the equipment. The experimental data obtained by thermal analysis (TG and DTG) were used to study the thermal decomposition kinetics of as-synthesized and purified CNT samples. Both the kinetic model and parameters were determined using the previously described model-fitting methods.

Textural characteristics of as-synthesized CNTs were determined by means of low temperature N_2 adsorption/desorption (LTNA) method, using He as a carrier gas (Micromeritics ASAP 2010). Mean pore diameter and pore volume were determined from desorption part of the N_2 isotherm and calculated by Barrett-Joyner-Halenda (BJH) method [21].

Results of decomposition kinetics

The thermal decomposition kinetic study of the examined CNT samples is based on the assumption of appropriate model giving the best fit of the obtained experimental data. In Fig. 1, the kinetic decomposition curves of the examined CNT samples are presented by way of conversion α as a function of T, as well as by taking a first derivate of the former ($d\alpha/dT$ versus α). As can be seen from Fig. 1b and d, all examined CNT samples are characterized by a bell-shaped $d\alpha/dT$ v.s. α function, characteristic of the following kinetic models: 2- and 3-dimensional diffusion models, chemical reaction models with a different reaction order, models of contracting area or volume and nucleation models (Table 1) [14]. Therefore, the experimental data were fitted to all feasible models, by taking their either differential or integral form of solution, $f(\alpha)$ or $g(\alpha)$, respectively, as given in Table 1. The validity of the model was confirmed according to the best statistical fit measured by a correlation coefficient. Consequently, two methods, the direct differential method (DDM) and the Coats-Redfern method (CRM) have been

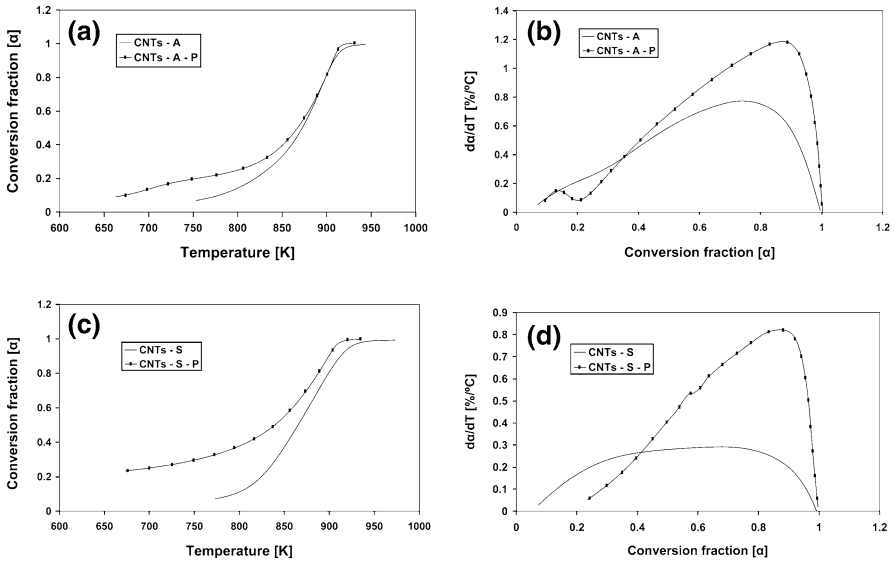

Fig. 1 Increment of conversion fraction (*left*) and rate of conversion (*right*) of as-synthesized and purified CNTs of different origin

Table 1 Selected thermal decomposition kinetic models having a sigmoidal geometry with the corresponding differential and integral forms [14]

Model	Differential form $f(\alpha) = 1/k\,\mathrm{d}\alpha/\mathrm{d}t$	Integral form $g(\alpha) = kt$
Avrami–Erofeyev(A2)	$2(1-\alpha)[-\ln(1-\alpha)]^{1/2}$	$[-\ln(1-\alpha)]^{1/2}$
Avrami–Erofeyev(A3)	$3(1-\alpha)[-\ln(1-\alpha)]^{2/3}$	$[-\ln(1-\alpha)]^{1/3}$
Avrami–Erofeyev(A4)	$4(1-\alpha)[-\ln(1-\alpha)]^{3/4}$	$[-\ln(1-\alpha)]^{1/4}$
Geometrical contraction models		
Contracting area (R2)	$2(1-\alpha)^{1/2}$	$1-(1-\alpha)^{1/2}$
Contracting volume (R3)	$3(1-\alpha)^{2/3}$	$1-(1-\alpha)^{1/3}$
Diffusion models		
2-D diffusion (D2)	$-[1/\ln(1-\alpha)]$	$((1-\alpha)\ln(1-\alpha))+\alpha$
3-D diffusion-Jander (D3)	$[3(1-\alpha)^{2/3}]/[2(1-(1-\alpha)^{1/3})]$	$(1-(1-\alpha)^{1/3})^2$
Ginstling-Brounshtein (D4)	$3/[2((1-\alpha)^{-1/3}-1)]$	$1-(2/3)\alpha-(1-\alpha)^{2/3}$
Reaction-order models		
First-order (F1)	$(1-\alpha)$	$-\ln(1-\alpha)$
Second-order (F2)	$(1-\alpha)^2$	$[1/(1-\alpha)]-1$
Third-order (F3)	$(1-\alpha)^3$	$(1/2)[(1-\alpha)^{-2}-1]$

applied. The DDM method uses the corresponding DTG data starting from the point of the CNTs onset temperature decomposition to the maximal point of decomposition rate $(d\alpha/dT)_{max}$, while the CRM method uses the same starting point, but the last one corresponds to the conversion fraction equal to 1. In Tables 2 and 3, the values of the correlation coefficients determined by fitting the experimental data in the above-mentioned 11 kinetic models are given.

Table 2 Correlation coefficient of experimental data fit into 11 kinetic models using the direct differential method

Model	Sample			
	CNTs-A R^2	CNTs-A-P R^2	CNTs-S R^2	CNTs-S–P R^2
D2	0.99311	0.98747	0.99044	0.94338
D3	0.98503	0.97081	0.99670	0.92100
D4	0.98745	0.99079	0.97201	0.94727
F1	0.97213	0.96723	0.99044	0.91741
F2	0.93888	0.92144	0.99890	0.86758
F3	0.91122	0.88713	0.99086	0.83116
R2	0.98799	0.99026	0.96857	0.94690
R3	0.98309	0.98323	0.97802	0.93692
A2	0.96402	0.97800	0.94902	0.93137
A3	0.95679	0.98229	0.90061	0.93752
A4	0.95070	0.98452	0.85621	0.94097

Table 3 Correlation coefficient of experimental data fit into 11 kinetic models using the Coats-Redfern method

Model	Sample			
	CNTs-A R^2	CNTs-A-P R^2	CNTs-S R^2	CNTs-S–P R^2
D2	0.98946	0.94136	0.99251	–*
D3	–	–	–	–
D4	0.98759	0.93566	0.99203	–
F1	0.97379	0.89283	0.98738	–
F2	0.94458	–	0.97537	–
F3	0.91122	–	0.95920	–
R2	–	–	–	–
R3	–	–	–	–
A2	0.96636	–	0.98473	–
A3	0.95814	–	0.98105	–
A4	0.93520	–	0.97565	–

* Obtained plot is not linear

A two-dimensional diffusion model (D2) during the thermal decomposition of CNTs-A sample might be speculated, as suggested by the results of the DDM calculation (Table 2). The model assumes a cylindrical shape of the solid particles, whereas the diffusion of the gas molecule (oxygen) occurs radially through the cylindrical shell [14]. The same CNTs-A sample gives the best statistical fit for the same model by applying the CRM as well (Table 3). The thermal decomposition rate of the same sample after purification (CNTs-A-P) is also controlled by a diffusion process, but in this case, the three-dimensional diffusion model (D4) appears to be the acting mechanism (Table 2). The application of the CRM gives another outcome (D2), however, with a low correlation coefficient indicating low reliability of occurrence of the model (Table 3). As for the CNT sample previously synthesized over SiO_2 supported catalyst (CNTs-S), second order kinetics (F2) is suggested by the DDM (Table 2). The fitting of the experimental data of thermal decomposition of the CNTs-S–P sample failed regardless of used method, either because of low correlation coefficients (DDM) (Table 2), or due to failure to achieve a linear relationship within any of the proposed models (CRM) (Table 3).

In general, for processing of the experimental data within all the tested kinetic models and for all examined CNT samples better fitting was achieved by using the DDM (Table 2). Accordingly, the kinetic parameters for all CNT samples were determined by using the same method and within the best fitted model, i.e. one with the highest value of the correlation coefficient in the series. Figure 2 shows the linear plots of Eq. 7 for the tested CNT samples within the models with the highest R^2 values, following to the appropriate kinetic parameters as presented in Table 4. In the case of thermal decomposition of CNTs-S sample, following the second-order kinetics (F2), the Freeman-Carroll method (FCM) can also be applied allowing for kinetic parameters verification (Fig. 3, Table 4).

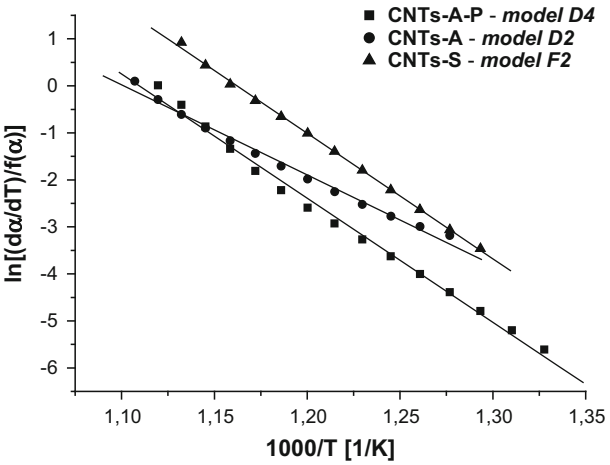

Fig. 2 Linear plot of CNT samples kinetic data obtained by DDM (Eq. 7)

Table 4 Kinetic parameters and correlation coefficients for thermal decomposition of the examined CNT samples using the direct differential and Freeman-Carroll methods

Sample	Method	*Ea* [kJ/mol]	*A* [K/min]	*n*	R^2	Model
CNTs-A	DDM	159.3	1.46×10^{10}	–	0.99311	D2
CNTs-A-P	DDM	219.5	5.26×10^{13}	–	0.99079	D4
CNTs-S	DDM	221.9	2.97×10^{14}	2.00	0.99890	F2
	FCM	205.9	–	1.50	0.99678	F2
CNTs-S–P[a]	–	–	–	–	–	–

DDM direct differential method, *FCM* Freeman-Carroll method

[a] Kinetic analysis using any of applied methods is not possible

Discussion

As shown in Table 4, the values of kinetic parameters are given only for three examined CNTs samples, while, for the CNTs-S–P sample none of the applied mathematical methods enabled a satisfactory fitting of the experimental data. The results of the previous DSC analysis revealed that both as-synthesized CNTs samples are characterized by similar values of the heat of combustion indicating their close thermal stability [12]. However, the lower onset temperature obtained for CNTs-A sample in DTG profiles indicates the existence of thinner tubes which start to decompose at lower temperature and thus the sample can be portrayed as of lower oxidation stability [12, 22]. This is in accordance with the determined values of CNTs activation energy obtained by DDM method (Table 4), which can be taken as an indicator of CNTs oxidation stability (159.3 kJ/mol for CNTs-A relative to 221.9 kJ/mol for the silica supported one) [23]. In addition, the presence of the compensation effect, showing higher number of active sites accounting for higher

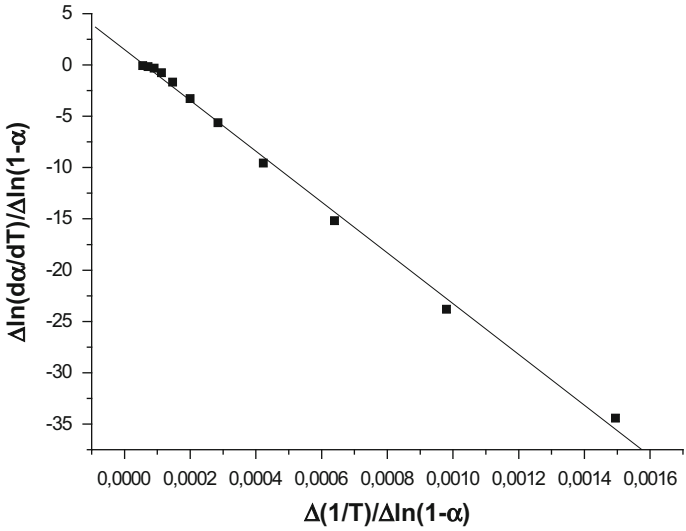

Fig. 3 Linear plot of CNTs-S sample kinetic data obtained by FCM (Eq. 10)

activation energy value, supports the plausibility of the calculated data. However, the analysis of kinetic curves showed that the rate of thermal decomposition of as-synthesized CNTs of different origin is controlled by different mechanisms: two-dimensional diffusion in the case of CNTs-A sample, specific for the solid particles of cylindrical shape, and the second order combustion in the case of CNTs-S sample. The validity of those as controlling kinetic steps were confirmed by the texture of the examined samples and by the satisfactory close values of activation energy and reaction order for the CNTs-S set of experimental data obtained by FCM (Table 4).

Different mechanisms that control the rate of as-synthesized CNTs thermal decomposition can be correlated with their textural characteristics. As can be seen from Fig. 4, CNTs-A sample is characterized by the dominating fraction of mesopores with the diameter values approaching the micropores (3-4 nm). On the other hand, the CNTs-S sample has a much higher proportion of larger pores, i.e. two dominating fractions with the maximum at 7 and 30 nm diameters. Therefore, the CNTs-A porous structure approaching the micro pore size can cause diffusion limitations, and accordingly, the rate of the thermal decomposition is controlled by the diffusion of O_2 molecules in the pores of the nanotubes.

The thermal decomposition kinetics of purified CNT samples is more complex relative to the as-grown ones, as the process mainly consists of a number of steps, wherein the rate of each is controlled by a different mechanism [8, 9]. These steps are due to formed/removed structural defects and CNTs functionalization degree upon purification and are characterized by the specific values of kinetic parameters [10, 11]. According to our previous results [12] both as-grown CNT samples have undergone the structural changes during purification. They have been subject to various oxidation degree during the purification process by the liquid oxidation in base/acid, resulting in different thermal stability, as well as the degree of functionalization. The higher

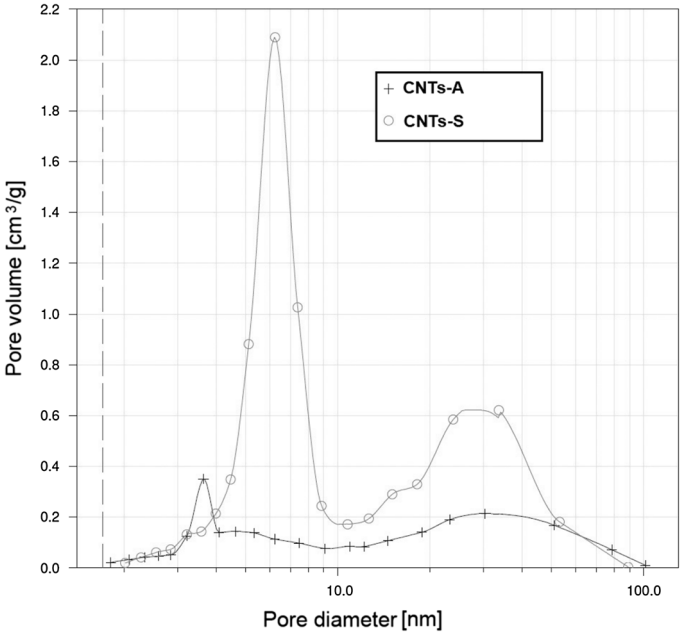

Fig. 4 Pore size distribution of as-synthesized CNT samples

activation energy of CNTs-A-P indicates higher oxidation stability of the purified sample, which may be due to an increased order degree of the samples structure, as well as its high concentration of hydrogen bonds. It is in accordance with the increased value of heat of combustion and high functionalization degree upon purification process found earlier by DSC and Raman spectroscopy [12]. The expected change in thermal properties after purification of the CNTs-S sample, however, cannot be validated, as any of the applied mathematical methods failed to describe the kinetic of its purified counterpart, CNTs-S–P. To do so, the study of thermal decomposition kinetics requires experimental data obtained by thermal analysis performed at different conditions, and also the application of several kinds of mathematical methods for processing the results.

Conclusion

The thermal decomposition kinetic parameters of as-grown and purified CNTs originating from alumina- and silica supported catalysts were determined using the selected model-fitting methods. The obtained results were correlated with the previously published ones showing thermal stability evolution of the tubes of different origin after the applied purification treatment. The values of activation energy and pre-exponential factor for as-grown CNTs are in accordance with their oxidation stability, while the different mechanism of their thermal degradation is a consequence of the

tubes specific textural characteristics. The kinetic parameters obtained for purified CNTs-A confirm the change of structural order degree after purification, speaking in favor of the procedure applied. On the other hand, the previously shown thermal stability variation for CNTs-S sample upon purification cannot be verified by any of the applied mathematical methods, suggesting the need of experimental data obtained by thermal analysis performed at different conditions.

Acknowledgments The financial support (Project 172059) of the Serbian Ministry of Education, Science and Technological Development is highly appreciated.

References

1. De Volder MFL, Tawfick SH, Baughman S, John Hart A (2013) Science 339:535
2. Sarkar S, Das PK, Bysakh S (2011) Mater Chem Phys 125:161
3. Chen Z-K, Yang J-P, Ni Q-Q, Fu S-Y, Huang Y-G (2009) Polymer 50:4753
4. Nie G, Zhang L, Cui Y (2013) React Kinet Mech Cat 108:193
5. Brukh R, Mitra S (2007) J Mater Chem 17:619
6. Illekova E, Csomorova K (2005) J Therm Anal Calorim 80:103
7. Vignes A, Dufaud O, Perrin L, Thomas D, Bouillard J, Janès A, Vallières C (2009) Chem Eng Sci 64:4210
8. Singh K, Hou X, Chou K-C (2010) Corros Sci 52:1771
9. Gallego J, Batiot-Dupeyat C, Mondragon F (2013) J Therm Anal Calorim 114:597
10. Chou YC, Hsieh TF, Hsieh YC, Lin CP, Shu CM (2010) J Therm Anal Calorim 102:641
11. Hsieh YC, Chou YC, Lin CP, Hsieh TF, Shu CM (2010) Aerosol Air Qual Res 10:212
12. Ratkovic S, Peica N, Thomsen C, Bukur DB, Boskovic G (2014) J Therm Anal Calorim 115:1477
13. Brown ME (2005) J Therm Anal Calorim 82:665
14. Khawam A, Flanagan DR (2006) J Phys Chem B 110:17315
15. Sharp JH, Wentworth SA (1969) Anal Chem 41:2060
16. Freeman ES, Carroll B (1958) J Phys Chem 62:394
17. Freeman ES, Carroll B (1969) J Phys Chem 73:751
18. Boonchom B (2009) J Therm Anal Calorim 98:863
19. Ratkovic S, Kiss E, Boskovic G (2009) CI&CEQ 15:263
20. Ratkovic S, Dj Vujicic, Kiss E, Boskovic G, Geszti O (2011) Mater.Chem. Phys. 129:398
21. Barrett EP, Joyner LG, Halenda PP (1951) J Am Chem Soc 73:373
22. McKee GSB, Vecchio KS (2006) J. Phys. Chem. B 110:1179
23. Sarkar S, Das PK (2012) J Therm Anal Calorim 107:1093